Single-index Open-phase Fault Detection Method for Six-phase Electric Drives

P. Entrambasaguas, I. González-Prieto, M.J. Duran

***Abstract*— Multiphase drives have the capability to continue operating when some phases are disconnected. This feature has been traditionally achieved with a reconfiguration of the control after the open-phase fault (OPF) occurrence. Since reconfiguration requires the localization of the faulty phase, different fault detection (FD) methods that use multiple indices have been proposed. A recent study suggests however that it is possible to achieve a passive/natural fault tolerance (FT) with no changes at the control stage. Since reconfiguration is avoided in the passive/natural approach, the localization of the open phase(s) is no longer needed. In this context, the control just requires the fault detection in order to apply the corresponding derating. This work suggests a single-index fault detection method that, together with the natural fault-tolerant control, provides enhanced robustness with minimum complexity. Experimental results confirm the possibility to detect the fault and distinguish between single and multiple OPFs using just one fault index.**

***Index Terms*— Fault detection, multiphase drives, model predictive control, fault tolerance.**

I. Introduction

One of the most distinctive features of multiphase drives is their capability to provide fault tolerance (FT) without additional hardware [1,4]. Their inherent redundancy allows achieving a smooth post-fault performance in the event of open-phase faults (OPFs) [5]. This fault tolerance is traditionally accomplished modifying the controllers [6], applying a mandatory derating [8] and recalculating the current references for maximum efficiency [7, 9,10,11], both with standard and alternative stator winding connections [12]. The enhanced reliability has been traditionally obtained in two stages:

- Stage 1 (S1): Fault detection and localization.
- Stage 2 (S2): Control reconfiguration.

In the conventional case, stage 1 requires both fault detection (action S1-1) and localization (action S1-2) of the specific faulty phases. In order to accomplish actions S1-1 and S1-2, several fault indices have been typically defined to determine whether the drive is operating normally or under OPFs. Many fault detection methods have been proposed in literature for three-phase drives [13-16]. Most of them use fault indices that are defined per phase, so they are fully re-usable for multiphase drives just extending the number of fault indices to the n phases.

However, some alternative approaches that are based on the vector space decomposition (VSD) of the n-dimensional space have also been suggested [17-19]. These methods are exclusive for multiphase systems because they use the x-y secondary components that simply do not exist in three-phase drives. Some benefits that include higher speed of detection and robustness have been reported for the OPF localization [18-19]. Regardless of approach, either per-phase or based on VSD, this stage requires at least n fault indices in order to localize the fault. Consequently, the complexity of the fault localizations grows with the number of phases.

Stage 2 obtains the information of the fault scenario from stage 1 and modifies the control scheme accordingly, typically performing three main actions:

- S2-1: Reconfiguration of the current references. The α-β and x-y currents are no longer independent, so it is necessary to modify the x-y current references to avoid conflicts [7-12].
- S2-2: Reconfiguration of the control structure. In most cases the pre-fault control structure does not suit the post-fault situation and it is necessary to modify the controllers [8-9].
- S2-3: Derating of the drive. The currents in the remaining healthy phases need to increase to compensate for the OPFs, hence it is necessary to derate the drive to avoid exceeding rated values that would eventually damage the motor [8-11].

The reconfiguration of the control structure depends on the regulation strategy. In standard field-oriented control (FOC) it is necessary to use proportional-resonant (PR) controllers instead to conventional proportional-integer (PI) controllers in order to cope with the non-constant post-fault x-y currents [8-9]. On the other hand, if the current loops are replaced by model predictive control (MPC) current regulators it is then necessary to modify the Clarke transformation and the cost function [20-21]. Regardless of the control approach, the FT is achieved at the expense of a higher overall complexity at the control stage.

Aiming to simplify stage 2, recent works suggests an alternative approach: designing a control structure that is valid both in pre- and post-fault situations [22-25]. This FT is referred as passive or natural because there is no need to modify the control scheme or the current references to obtain a smooth post-fault performance. All previous FT proposals required at least the mandatory modification of S2-1 (recalculation of the current references), and in different cases the modification of the controllers (S2-2) [6-12, 20-21]. In other words, the natural FT fully avoids modifications S2-1 and S2-2. As a result, the drive automatically operates after the OPF occurrence with a satisfactory performance. This concept has been introduced in [22] for an MPC based on the inclusion of synthetic/virtual voltage vectors (termed VVs in what follows). The VV-MPC allows performing the x-y current control in open-loop mode, hence avoiding the controllers conflict in post-fault situation. As a consequence, the natural FT highly simplifies stage 2.

Manuscript received June 30, 2019; revised August 28, 2019; accepted November 22, 2019.

This research was funded by the Spanish Government under the Plan Estatal 2017-2020 with the reference RTI2018-096151-B-I00.

P. Entrambasaguas, I. Gonzalez-Prieto and M.J. Duran and are with the Department of Electrical Engineering at the University of Malaga, Spain, e-mail: paulaentrambasaguas@gmail.com, ignaciogp87@gmail.com and mjduran@uma.es.

Although the natural FT is automatically achieved (action S2-1 and S2-2 are avoided), it is still necessary to apply the drive derating (action S2-3) in order to keep the drive safe in prolonged operation. The degree of drive derating is a solved issue that is extensively covered in [8], but the application of this derating mandatorily requires to identify the fault scenario. However, the localization of the specific phases under OPF, which was mandatory for S2-1, is no longer required. For the sake of example, the degree of derating in S2-3 is the same in all single OPFs for symmetry considerations [8]. This opens the possibility to also simplify stage 1. While the determination of the faulty phases requires the use of at least n fault indices [18-19], this works suggest a simplified fault detection method that only requires one fault index. The main idea behind the method is that, regardless of the specific faulty phase(s), any OPF increases the value of the x-y currents. Since the machine has distributed windings, the x-y currents are driven close to zero in normal operation of the drive for efficiency reasons. Nevertheless, when the OPF occurs, the x-y currents are inevitably linked to the α-β currents. Since the machine is supplied with non-null α-β currents, the x-y currents also become non-zero regardless of the OPF scenario.

The proposed FD method together with the natural FT strategies provide a fault-tolerant drive with minimum complexity. Specifically, only fault detection (with a single fault index) and derating is required to provide the electric drive with a self-healing capability. The fault localization (action S1-2), current references modification (action S2-2) and control reconfiguration (action S2-3) are skipped. In this work the proposed single-index FT method has been tested it using a natural FT strategy that is based on MPC current controllers with VVs. Once the OPF scenario is detected with the proposed fault detection method, the degree of derating is taken from [8] and applied to preserve the integrity of the drive.

The paper is structured as follows. Section II briefly describes the VV-MPC control scheme. Section III details the proposed single-index FD method and analysis the different independent fault scenarios. Section IV experimentally tests the proposed FD method under single and double OPFs, and section V finally draws the main conclusions of the study.

II. Model Predictive Control with Natural Fault Tolerance in Six-phase Induction Motor Drives

A. Six-phase induction motor drives

The topology that is used hereafter in this work consists of an asymmetrical six-phase induction machine (IM) fed by two three-phase two-level voltage source converters (VSC), as shown in Fig. 1. The selected asymmetrical IM has distributed windings and it is formed by two sets of three-phase windings spatially shifted 30 degrees and connected to two isolated neutral points. The VSCs are supplied from a single dc-link, providing 2^6=64 switching states. These switching possibilities have been traditionally expressed using a vector S=$[S_{a1}\ S_{b1}\ S_{c1}\ S_{a2}\ S_{b2}\ S_{c2}]^T$ whose elements S_{ij} are binary coded, i.e. $S_{ij}=0$ when the upper switch of the leg is OFF and $S_{ij}=1$ if the upper switch is ON. This vector $[S]$ can be employed to obtain the phase voltage vectors:

$$\begin{bmatrix} v_{a1} \\ v_{b1} \\ v_{c1} \\ v_{a2} \\ v_{b2} \\ v_{c2} \end{bmatrix} = \frac{Vdc}{3} \begin{bmatrix} 2 & -1 & -1 & 0 & 0 & 0 \\ -1 & 2 & -1 & 0 & 0 & 0 \\ -1 & -1 & 2 & 0 & 0 & 0 \\ 0 & 0 & 0 & 2 & -1 & -1 \\ 0 & 0 & 0 & -1 & 2 & -1 \\ 0 & 0 & 0 & -1 & -1 & -2 \end{bmatrix} \begin{bmatrix} S_{a1} \\ S_{b1} \\ S_{c1} \\ S_{a2} \\ S_{b2} \\ S_{c2} \end{bmatrix} \quad (1)$$

Different reference frames have been proposed in the literature to simplify the modeling process of IMs. For that purpose, the power-invariant Clarke transformation matrix can be employed to express the phase variables in two orthogonal stationary subspaces (α-β and x-y), plus two zero-sequence components (0_+ and 0_-):

$$[T] = \frac{1}{\sqrt{3}} \begin{bmatrix} 1 & -1/2 & -1/2 & \sqrt{3}/2 & -\sqrt{3}/2 & 0 \\ 0 & \sqrt{3}/2 & -\sqrt{3}/2 & 1/2 & 1/2 & -1 \\ 1 & -1/2 & -1/2 & -\sqrt{3}/2 & \sqrt{3}/2 & 0 \\ 0 & -\sqrt{3}/2 & \sqrt{3}/2 & 1/2 & 1/2 & -1 \\ 1 & 1 & 1 & 0 & 0 & 0 \\ 0 & 0 & 0 & 1 & 1 & 1 \end{bmatrix} \quad (2)$$

$$[v_{\alpha s}\ v_{\beta s}\ v_{xs}\ v_{ys}\ v_{0+}\ v_{0-}]^T = [T][v_{a1}\ v_{b1}\ v_{c1}\ v_{a2}\ v_{b2}\ v_{c2}]^T$$

where α-β components are related with the flux/torque production and x-y components only produce stator copper losses in the case of distributed-winding machines. Fig. 2 shows the localization of voltage vectors in the α-β and x-y planes, where a decimal number equivalent to the binary codification of $[S]$ has been used to identify the corresponding voltage vector.

Based on the previous approach, the differential equations of a six-phase IM can be expressed using vector space decomposed (VSD) variables as follows:

$$\begin{aligned} v_{\alpha s} &= \left(R_s + L_s\frac{d}{dt}\right) i_{\alpha s} + M\frac{d}{dt} i_{\alpha r} \\ v_{\beta s} &= \left(R_s + L_s\frac{d}{dt}\right) i_{\beta s} + M\frac{d}{dt} i_{\beta r} \\ v_{xs} &= \left(R_s + L_{Ls}\frac{d}{dt}\right) i_{xs} \\ v_{ys} &= \left(R_s + L_{Ls}\frac{d}{dt}\right) i_{ys} \\ 0 &= \left(R_r + L_r\frac{d}{dt}\right) i_{\alpha r} + \omega_r L_r i_{\beta r} + M\frac{d}{dt} i_{\alpha s} + \omega_r M i_{\beta s} \\ 0 &= -\omega_r L_r i_{\alpha r} + \left(R_r + L_r\frac{d}{dt}\right) i_{\beta r} - \omega_r M i_{\alpha s} + M\frac{d}{dt} i_{\beta s} \\ T_e &= PM\left(i_{\alpha s} i_{\beta r} - i_{\beta s} i_{\alpha r}\right) \end{aligned} \quad (3)$$

where $L_s = L_{ls} + 3 \cdot L_m$, $L_r = L_{lr} + 3 \cdot L_m$, $M = 3 \cdot L_m$ and ω_r is the rotor electrical speed ($\omega_m = P \cdot \omega_r$, being P the pole pair number). Indices s and r denote stator and rotor variables and subscripts l and m indicate leakage and magnetizing inductance, respectively.

B. Model Predictive Control Using Virtual Voltage Vectors

MPC based on VVs maintains the outer proportional-integral (PI) controller for the speed regulation and the inner predictive current regulators of standard MPC [26-27]. However, a reduced machine model/cost-function can be employed because the standard voltage vectors are replaced by virtual voltage vectors. Fig. 3 shows an MPC scheme for a six-phase IM where VVs are implemented.

As described in [22], the inclusion of VVs into an MPC scheme allows performing the x-y current regulation in open-loop mode. For that purpose, VVs must be determined offline using pairs of medium-large (turquoise diamonds in Fig. 2) and large (purple pentagons in Fig. 2) voltage vectors with the same direction in the α-β plane. Fortunately, the abovementioned voltage vectors couples have opposite directions in the x-y plane (see Fig. 2) and therefore allow to obtain active α-β voltage and null average value of the x-y

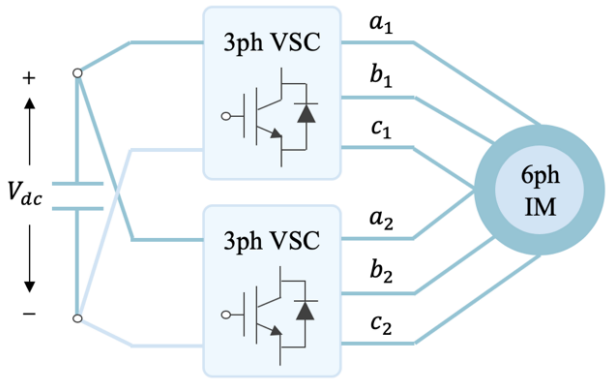

Fig. 1. Scheme of a six-phase IM with two VSCs connected to a single dc-link.

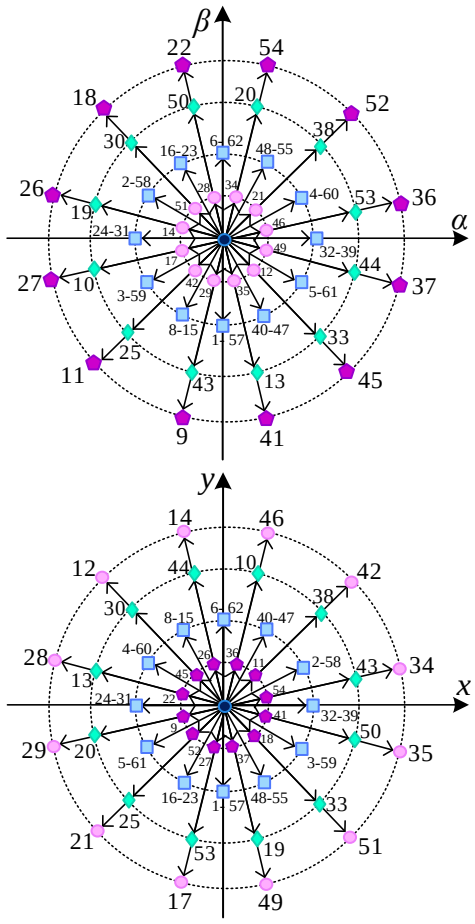

Fig. 2. Stator voltage vectors in α-β and x-y planes.

voltages. This is achieved using different application times for the large and medium-large vectors. Following this procedure, 12 active virtual voltage vectors can be defined as:

$$VV_i = t_1 \cdot V_{large} + t_2 \cdot V_{medium-large} \quad (4)$$

where t_1 and t_2 are application times for each voltage vector ($t_1 = 0.73 \cdot T_m$ and $t_2 = 0.27 \cdot T_m$ for the selected topology) and T_m represents the sampling time. Fig. 4 shows the VVs localization in the α-β plane. These VVs have a magnitude that is 92% the amplitude of large vectors in the α-β and allow regulating the x-y currents in open-loop mode [22].

VV-MPC presents some differences compared to standard MPC. From the point of view of the machine model, a reduced machine model without x-y components can be employed, since the regulation of these components is directly provided in open-loop mode by the VVs. The following machine model can accordingly be defined:

$$\frac{d}{dt}[X_{\alpha\beta}] = [\bar{A}] \cdot [X_{\alpha\beta}] + [\bar{B}] \cdot [U_{\alpha\beta}]$$
$$[Y_{\alpha\beta}] = [\bar{C}] \cdot [X_{\alpha\beta}] \quad (5)$$

where

$$[U_{\alpha\beta}] = [u_{\alpha s}\ u_{\beta s}\ 0\ 0]^T$$
$$[X_{\alpha\beta}] = [i_{\alpha s}\ i_{\beta s}\ i_{\alpha r}\ i_{\beta r}]^T \quad (6)$$
$$[Y_{\alpha\beta}] = [i_{\alpha s}\ i_{\beta s}\ 0\ 0]^T$$

where matrices $[\bar{A}]$, $[\bar{B}]$ and $[\bar{C}]$ define the dynamics of a six-phase IM and their coefficients are dependent on the machine parameters [24].

The same approach can be employed for the cost function and therefore a reduced cost function can be defined without x-y current terms:

$$J_K = K_\alpha \cdot (i_\alpha^* - \hat{\imath}_\alpha)^2 + K_\beta \cdot \left(i_\beta^* - \hat{\imath}_\beta\right)^2 \quad (7)$$

where K_α and K_β are the weighting factor of the reduced cost-function.

To summarize, VV-MPC allows minimizing the MPC performance degradation due to low values of the stator leakage inductance and, at the same time, reduces the computational cost. Moreover, this MPC version avoids the controllers' conflict in post-fault situation since the x-y current regulation is realized in open-loop mode. Therefore, the control scheme can provide fault tolerance without any control reconfiguration, as it is described next.

C. Natural Fault Tolerance

OPFs have been the most studied post-fault situations in the literature of multiphase drives [3-12]. Several OPF localization methods and post-fault controllers have been developed in last decade in order to provide OPF tolerance [3-12,17-19]. However, [22] recently introduced the concept of natural fault against OPF in multiphase drives regulated using VV-MPC, where the post-fault control reconfiguration is no longer necessary.

The abovementioned controllers' conflict is caused by the new post-fault constraint of the system. The current cannot flow through the damaged phase when an open-phase fault occurs. For that reason, a new constraint appears in the system and, therefore, α-β and x-y planes are no longer independent. This new condition can be known applying the fault condition to the inverse of the Clarke transformation matrix (2). Thus, for the selected topology when an OPF appears in phase a_1, the new constrain in the system is:

$$i_x = -i_\alpha \quad (8)$$

As a consequence, α-β and x-y controllers have incompatible objectives in this new situation: α-current needs to be drive to non-null values to provide the necessary flux/torque, whereas x-current still aims to be drive to zero. This conflicting situation has been traditionally solved with the reconfiguration of the control according to the specific OPF localization. However, this controllers' conflict can be avoided if x-y current regulation is realized in open-loop mode [22, 24-25].

As previously exposed, for the case of MPC the use of VVs allows doing the control of x-y currents in open-loop mode and therefore a natural fault tolerance against OPF is obtained with their implementation.

.

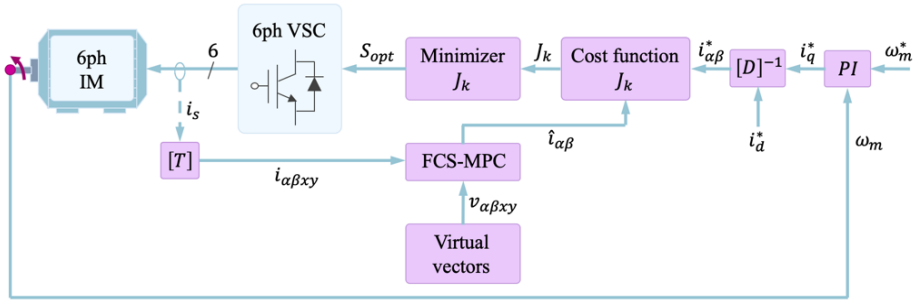

Fig. 3. VV-MPC scheme for a six-phase IM.

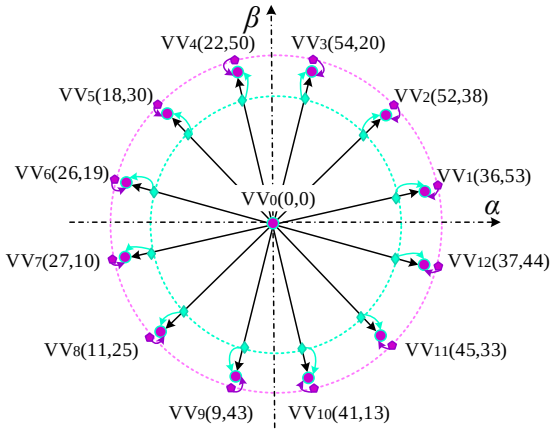

Fig. 4. Virtual voltage vectors for six-phase IMs.

III. Single-index Fault Detection Method and Fault Scenarios.

A. *Single-index fault detection method*

The natural FT from the formerly described VV-MPC does not require the localization of the fault because the control modifications S2-1 and S2-2 (current references and control reconfiguration) are no longer needed. Nevertheless, there are two main requirements for the application of the drive derating (i.e. modification S2-3):

R1) Open-phase fault detection.

R2) Identification of the fault scenario.

It is known that, regardless of the type of fault, the secondary x-y currents become non-zero after the OPF occurrence. Hence, a simple manner to detect an OPF (requirement R1) is to monitor the relative value of the x-y currents with respect to the α-β currents. For this purpose, this work suggests the use of the following fault index:

$$R = \frac{i_x^2 + i_y^2}{i_\alpha^2 + i_\beta^2} \tag{9}$$

Conceptually, when the fault index R from (9) is close to zero the drive would be operating in healthy mode, whereas the machine would be under OPF when R is different from zero. In practice, x-y currents can have a significant ripple due to the low impedance in the secondary plane, so the fault index R will also present some ripple. Furthermore, eventual spikes in the current measurements may lead to false alarms in the FD process

While in the fault detection suggested in [18] it is necessary to use n fault indices (one per phase), a single index is proposed in (9) in order to identify the fault scenario with a higher simplicity.

In order to avoid eventual false alarms due to instantaneous inaccurate values, a moving average is applied to the fault index from (1), obtaining the averaged value:

$$\bar{R} = \frac{1}{T_m}\int_{t-T_m}^{t} R(t)dt \tag{10}$$

where T_m is the period of the moving window that is used for the FD. High values of T_m lead to slow FD with low $\bar{R}$ ripple whereas low values of T_m accelerates the FD at the expense of a lower robustness. Unlike methods with control reconfiguration, the detection time is not critical because the immediate switch to a post-fault scheme is no longer necessary. For this reason, the period T_m is always set to be at least equal to one fundamental period:

$$T_m = \sigma \cdot \hat{T}_s, \quad \sigma \geq 1 \tag{11}$$

where:

$$\hat{T}_s = \frac{2\pi}{\hat{\omega}_s} \quad with \quad \hat{\omega}_s = \frac{i^*_{qs}}{\tau_r \cdot i^*_{ds}} + P \cdot \omega_m \tag{12}$$

where $\tau_r = L_r/R_r$ is the rotor time constant, and i^*_{ds} and i^*_{qs} are the d-q current references taken from the control.

The use of a moving window is a common procedure both in three-phase [14-16] and multiphase [18-19] fault localization methods and makes the FD stage more stable.

On the other hand, with regard to the ripple that can present $\bar{R}$, it is necessary to define a certain threshold to provide a security margin. This threshold depends on the x-y current ripple and must be experimentally determined to find a tradeoff between robustness and accuracy. Monitoring if the averaged value $\bar{R}$ is below or above the predefined threshold, the FD becomes feasible (Fig. 5).

B. *Open-phase faults scenarios*

Nevertheless, the derating is not the same in all fault scenarios, hence the application of a single threshold cannot satisfy requirement R2. For derating purposes, there are only three independent sets of scenarios in a six-phase machine with two isolated neutrals:

F1) Set of single OPFs, including one OPF in any of the six phases.

F2) Set of double OPFs (case 1), including two OPFs produced either in the same set of windings or in different ones with a phase shift of 90°.

F3) Set of double OPFs (case 2): including two OPFs in windings from different sets with a phase displacement of either 30° or 150°.

For derating purposes and based on symmetry considerations, it is the same if the OPF occurs in phase a_1 or b_2 because all single OPFs belong to set F1. Since the natural fault tolerance detailed in section II.C can be achieved without any control reconfiguration, the knowledge about the specific faulty phases is not necessary.

Based on the aforementioned OPFs scenarios, it is possible to calculate the theoretical value of the fault index defined in (9). Assuming that the α-β currents maintain their circle

shape in post-fault situation using VV-MPC, they can be defined as follows:

$$i_\alpha(t) = I_n \cdot \cos(\omega_s \cdot t)$$
$$i_\beta(t) = I_n \cdot sin(\omega_s \cdot t) \quad (13)$$

where I_n is the amplitude of the α-β currents and ω_s is the stator frequency.

On the other hand, using the fault locator indices proposed in [18] the x-y currents can be expressed as a function of the α-β currents for each specific OPF scenario. Therefore, for the case of a single OPF in the phase a_1 (F1 scenario), the constraint defined in (8) appears in the system. Based on (13) and the fault restriction, the x-current can be defined as:

$$i_x(t) = -I_n \cdot \cos(\omega_s \cdot t) \quad (14)$$

Since there is still a degree of freedom in the system, the y-current can be maintained equal to zero to achieve minimum copper losses in this OPF scenario:

$$i_y(t) = 0 \quad (15)$$

Finally, introducing the modules of theoretical α-β and x-y currents in (9), the value of $\bar{R}$ over an electrical cycle is:

$$\bar{R} = \frac{i_x^2 + i_y^2}{i_\alpha^2 + i_\beta^2} = \frac{0.5 \cdot T_s \cdot I_n^2}{T_s \cdot I_n^2} = 0.5 \quad (16)$$

Since the six-phase IM behavior is symmetric for single OPF [20], this value of R can be employed to identify all fault scenarios from set F1 (single OPFs).

Following the same procedure, the value of R can also be calculated for F2 scenario. Taking the restriction due to a double open-phase fault in phase a_1 and c_2 the theoretical value of R can be obtained for F2 scenario. According to abovementioned post-fault situation, x-y currents are [18]:

$$i_x(t) = -I_n \cdot \cos(\omega_s \cdot t)$$
$$i_y(t) = -I_n \cdot sin(\omega_s \cdot t) \quad (17)$$

Finally, introducing the modules of theoretical α-β and x-y currents in (9), the theoretical value of $\bar{R}$ calculated over an electrical cycle is:

$$\bar{R} = \frac{i_x^2 + i_y^2}{i_\alpha^2 + i_\beta^2} = \frac{T_s \cdot I_n^2}{T_s \cdot I_n^2} = 1 \quad (18)$$

The same approach can be employed again for F3 scenario. However, Scenario F3 can also be simply identified when the fault index $\bar{R}$ is above the theoretical value of scenario F2.

In order to illustrate the behavior of the currents in post-fault situation for the proposed fault scenarios, Fig. 6 shows the α-β and x-y current diagram for the different OPF scenarios when $|i_{\alpha\beta}|$=1 A. It can be observed the degree of severity that corresponds to each OPF scenario (e.g. Fig. 6c shows very high x-y currents).

As a summary, although the number of single and double fault scenarios is equal to $n + n \cdot (n-1)/2$ (i.e. 21 for $n = 6$), only three different derating values need to be applied after the OPF. The lowest derating is found in set F1, whereas the higher derating corresponds to set F3. A detailed analysis of the derating can be found in [8] for different configurations in six-phase IMs. It is then expected that the value of the fault index $\bar{R}$ will also differ in scenarios. Aiming to satisfy the requirement R2, it is possible to define three different thresholds for each set of fault scenarios (T_h^{F1}=0.3, T_h^{F2}=0.8 and T_h^{F3}=1.2). The values of theses thresholds have been estimated in order to avoid false alarms in healthy mode and provide a suitable detection speed. Following this procedure, the drive state can be determined with a single fault index:

- Healthy mode: the fault index $\bar{R}$ is below T_h^{F1}.
- Single OPF (F1): the fault index $\bar{R}$ is above T_h^{F1} and below T_h^{F2}.
- Double OPF case 1 (F2): the fault index $\bar{R}$ is above T_h^{F2} and below T_h^{F3}.
- Double OPF case 2 (F3): the fault index $\bar{R}$ is above T_h^{F3}.

Fig. 5 depicts the aforementioned states and how the FD procedure can differentiate between them with just the single index $\bar{R}$.

It is worth noting here that the use of the proposed single-index FD method together with the natural FT control approach highly simplifies the design of the FT drive compared to the standard case when the fault needs to be localized and the control requires reconfiguration. Table I performs a qualitative comparison that clarifies how the proposed solution reduces the overall complexity and provides higher robustness, hence improving the prospect for industry applications.

IV. Experimental results.

A. Test Bench

The performance of the proposed single index FD method has been evaluated in the test bench of Fig.7. In this experimental ring, a custom-built asymmetrical six-phase machine is fed by two commercial VSCs (Semikron SKS22F modules). These VSCs are connected to a single dc-link supplied with a single dc-power (LAB/HP 15300/0-300V/0-50A). Table II provides the information of the electric drive, where the IM parameters have been estimated using two different standard estimation techniques [28-29].

The six-phase IM is loaded coupling its shaft to a dc-machine. The armature of the dc-machine is connected to a variable resistive load that dissipates the power, therefore the load is speed-dependent. The dc-machine shaft is coupled to a digital encoder (GHM510296R/2500) to measure the rotational speed of the drive. From the control point of view, phase currents also need to be obtained, and for that purpose four hall-effect sensors installed in the VSCs are employed (LEM LAH 25-NP). A digital signal processor (TMS320F28335 from Texas Instruments, TI) receives the adapted signals of the abovementioned sensors and realizes the control actions.

B. Experimental results

Four set of tests have been designed to confirm that the proposed FD method (Fig. 5) can successfully satisfy requirements R1 an R2:

- Test set 1: the machine is operated in steady-state condition when a single OPF (F1) occurs at $t = 10\ s$.
- Test set 2: the machine is operated in steady-state condition when a double OPF (F2) occurs at $t = 10\ s$.
- Test set 3: the machine is operated in steady-state condition when a double OPF (F3) occurs at $t = 10\ s$.
- Test set 4: the proposed fault detection method is evaluated under different operating conditions.

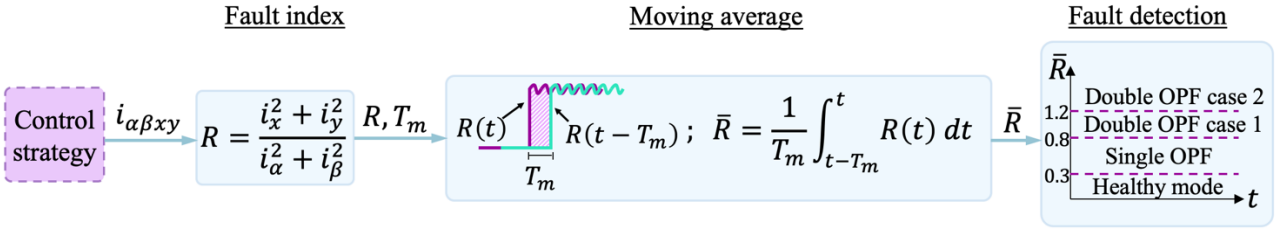

Fig.5. Single-index fault detection method for natural FT control strategies

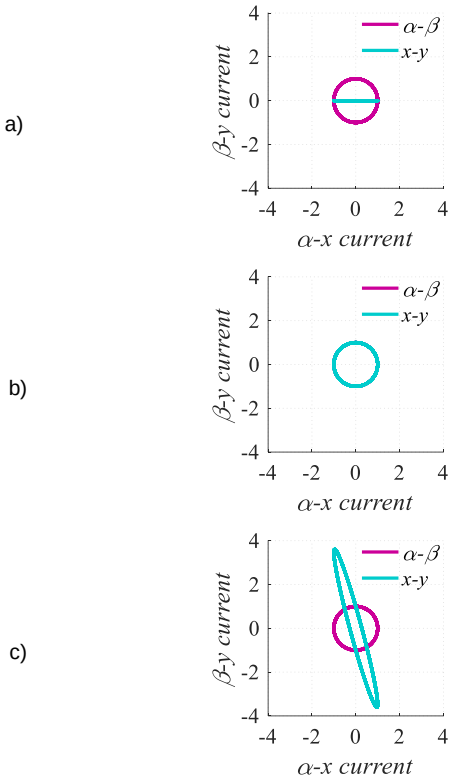

Fig. 6. α-$\beta$and x-y currents diagram for: a) F1 scenario (OPF in phase a_1), b) F2 scenario (OPFs in phases a_1 and c_2) and c) F3 scenario (OPFs in phases a_1 and b_2).

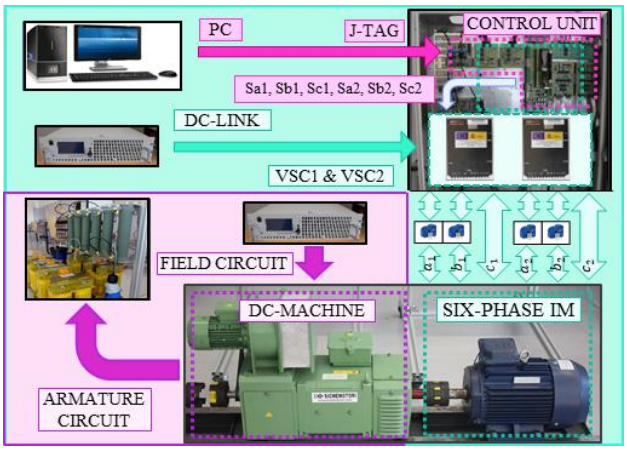

Fig. 7. Tech bench.

In the three first sets of tests the machine is driven at 300 rpm with a load torque of 4 Nm in pre-fault condition and the OPFs are provoked with a relay that fully disconnects the IM terminal from the VSC. The values of the single fault index $\bar{R}$ for fault scenarios F1, F2 and F3 are expected to be 0.5, 1 and > 1, respectively. For this reason, the thresholds T_h^{F1}, T_h^{F2} and T_h^{F3} are set to intermediate values of 0.3, 0.8 and 1.2. Experimental tests from sets 1 to 3 confirm in any case the theoretical values of the fault index $\bar{R}$ in all possible scenarios.

Fig. 8 shows two single OPF scenarios for phases a_1 and c_2. In both cases the currents are increased and become unbalanced after the OPF occurrence. The fault index $\bar{R}$ is close to zero when the drive is healthy (before $t = 10\ s$) and the eventual spikes are far from the threshold $T_h^{F1} = 0.3$. This confirms the lack of false alarms in pre-fault situation. Conversely, after the single OPF occurrence, the fault index $\bar{R}$ evolves to the theoretical value of 0.5 from (16) (see Fig. 8), which is in between $T_h^{F1} = 0.3$ and $T_h^{F2} = 0.8$. At this time the OPF is detected and the fault scenario is correctly identified as belonging to scenario F1 (i.e. single OPF). Although, the control structure does not require any modification, the fault detection and the identification allow applying the corresponding derating (see [8] for details on the calculation of the derating values). Both in pre- and post-fault situations the fault index $\bar{R}$ successfully remains within the correct zone with a margin of security that guarantees the robustness of the proposed single-index FD method.

Fig. 9 shows the cases of two double OPFs (F2), corresponding to phases a_1-c_1 and b_1-a_2. In both cases the fault index $\bar{R}$ remains below $T_h^{F1} = 0.3$ in pre-fault situation and evolves to 1 after the fault occurrence. This unity value was already expected according to the waveform of the α-β and x-y currents (i.e. equal circular shape, as shown in Fig. 6). Since the unity value is located within $T_h^{F2} = 0.8$ and $T_h^{F3} = 1.2$, the fault is correctly identified to be in scenario F2. Again, both the pre- and post-fault states can be identified with a sufficient margin to avoid false alarms and to apply the corresponding derating after the fault.

Fig. 10 shows the cases of two double OPFs (F3), corresponding to phases a_1-a_2 and b_1-c_2. The evolution of the fault index $\bar{R}$ is similar to the previous cases: it is close to zero in healthy operation and increases after the fault occurrence. Nevertheless, in this case the spatial location of the faulty phases is particularly unfavorable (e.g. phases a_1 and a_2 are both located in the same region) and this highly elevates the necessary derating and the fault index value. When the values of $\bar{R}$ are over 1, fault scenarios corresponding to set F3 are clearly identified because the value of $T_h^{F3} = 1.2$. It is worth highlighting once more that the proposed FD procedure can simultaneously detect the fault and also identify if the fault scenario belongs to F1, F2 or F3 with a sufficient security margin.

Finally, Fig. 11 shows the performance of the proposed single index for the same open-phase fault (phase a_1) at different operating points. Fig. 11a validates the performance of the proposed $\bar{R}$ index when the reference speed is 600 rpm and the load torque is 4 Nm, whereas Fig 11b shows the performance of $\bar{R}$ when the refence speed is 200 rpm with no load torque. It can be observed that, regardless of the operating conditions, the proposed single index increases when the open-phase fault occurs, allowing the successful identification of the anomalous situation.

TABLE I
FAULT DETECTION AND FAULT-TOLERANT CONTROL COMPARISON

	Reconfigured FT control with fault localization	Natural FT control with single-index fault detection
Fault detection and identification (S1-1)	✓	✓
Fault localization (S1-2)	✓	–
Number of fault indices	$> n$	1
Current references recalculation (S2-1)	✓	–
Control reconfiguration (S2-2)	✓	–
Application of the current derating	✓	✓
Fault scenarios to be considered for single and double faults	$n + \frac{n \cdot (n-1)}{2}$	–
High overall complexity	✓	–
Impact of FD errors/ delays on the FT control performance	✓	–

TABLE II
SIX-PHASE IM AND DRIVE PARAMETERS

Parameters	Values	Units
Stator resistance, R_s	14.2	Ω
Rotor resistance, R_r	2.04	Ω
Stator leakage inductance, L_{ls}	1.5	mH
Rotor leakage inductance, L_{lr}	55	mH
Mutual inductance, M	420	mH
Number of pole pairs, P	3	-
Nominal current, i_{q_max}	3.5	A
Rated torque, T_n	8.3	N·m
Sampling frequency, f_m	7.5	kHz
dc-link, V_{dc}	200	V

Since the set of tests 1 to 3 shown in Figs. 8-10 cover all possible scenarios, it can be concluded that a single index serves to satisfy requirements R1 and R2. Moreover, test 4 has confirmed the capability of the proposed fault detection method to identify fault scenarios for different operating conditions. Consequently, the proposed single-index FD method can be successfully used together with natural FT strategies. The combination of the single-index FD and natural FT control provides a simple and robust manner to allow the operation of multiphase drives in the event of OPF (see table I).

V. CONCLUSIONS.

Although conventional procedure to provide fault tolerance to multiphase machines is feasible, its complexity grows with the number of phases. The minimum number of fault indices for fault localization is n and the number of single and double fault scenarios to accomplish the control reconfiguration is $n + n \cdot (n-1)/2$.

An alternative approach has been recently presented that provides fault tolerance in a natural manner, i.e. without any action on the control strategy (except the derating of the drive). Nevertheless, the higher simplicity is restricted to the control stage, whereas the complexity of the fault detection remains the same so far.

Since the natural FT does not require the localization of the specific phases under OPF, it is demonstrated in this work that it is possible to detect the fault using a single fault index instead of the multiple indices ($\geq n$) required in previous works.

The proposed single-index FD method does not only detect the fault, but also provides information about the fault scenario (single OPF, double OPF case 1 or double OPF case 2). Hence, with a single fault index it is possible to extract the necessary information (i.e. the distinction between fault scenarios F1, F2 and F3) to appropriately derate the drive after the OPF occurrence.

The joint use of the single-index FD method and the natural FT control make the drive tolerant to OPFs with minimum steps and reduced complexity.

REFERENCES

[1] E. Levi, F. Barrero, and M.J. Duran, "Multiphase machines and drives – Revisited," *IEEE Trans. Ind. Electron.*, vol. 63, no. 1, pp. 429–432, Jan. 2016.

[2] E. Levi, "Advances in converter control and innovative exploitation of additional degrees of freedom for multiphase machines," *IEEE Trans. Ind. Electron.*, vol 63, no. 1, pp. 433–448, Jan. 2016.

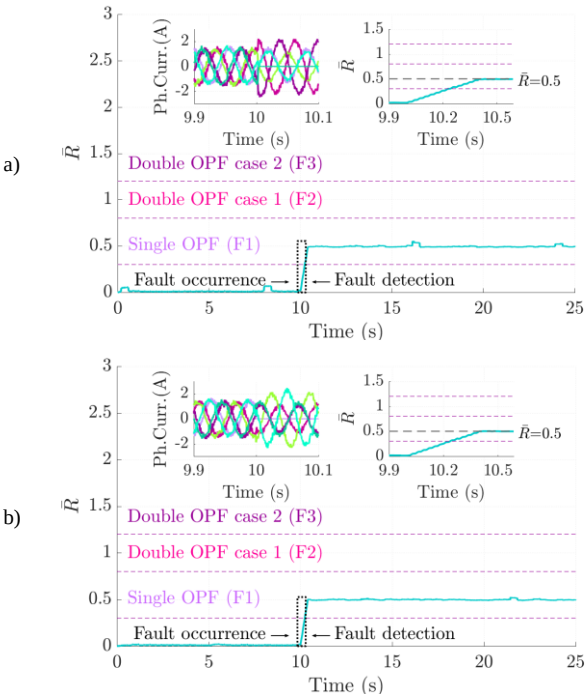

Fig. 8. Evolution of the fault detection index in the proposed method in the scenario F1 for: a) a_1 and b) c_2, at $t = 10s$.

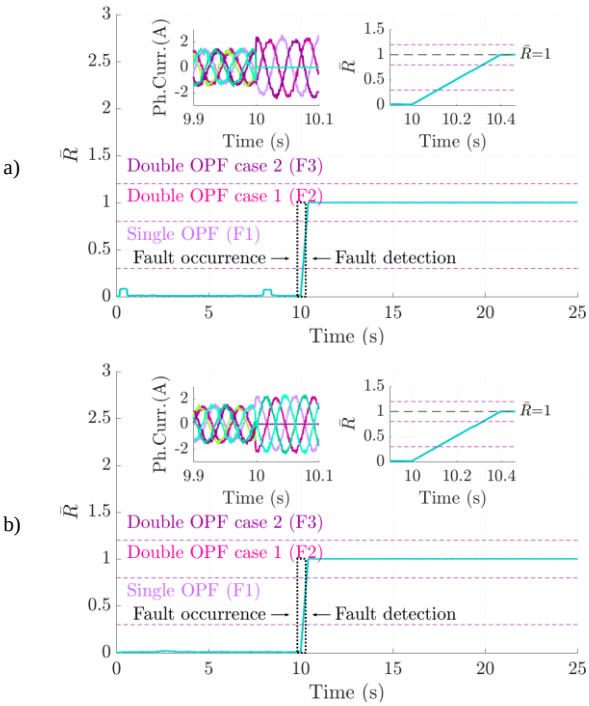

Fig. 9. Evolution of the fault detection index in the proposed method in the scenario F2 for: a) a_1-c_1 and b) b_1-a_2, at $t = 10s$.

a)

b)

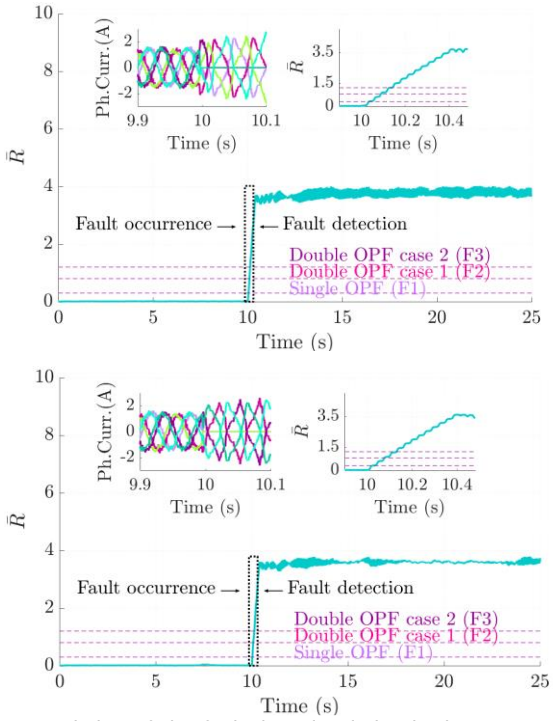

Fig. 10. Evolution of the fault detection index in the proposed method in the scenario F3 for: a) a_1-a_2 and b) b_1-c_2, at $t = 10s$.

a)

b)

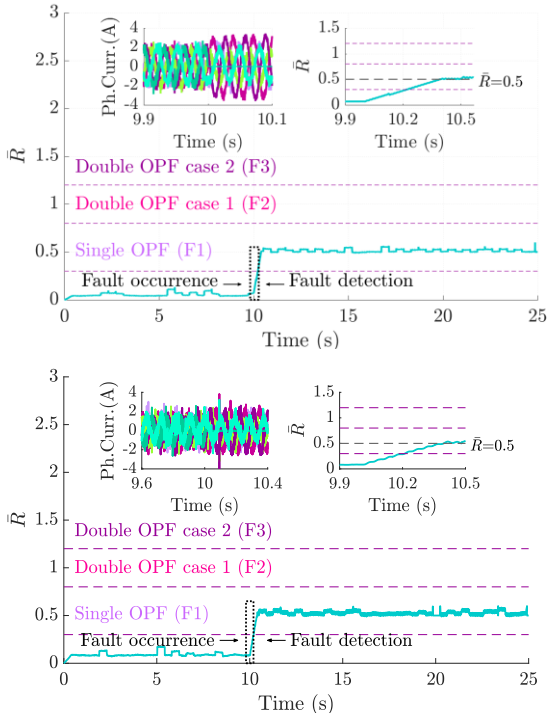

Fig. 11. Evolution of the fault detection index in the proposed method in the scenario F1 for: a) OPF in a_1 with high speed/load and b) a_1 with low speed/load, at $t = 10s$.

[3] F. Barrero and M.J. Duran, "Recent advances in the design, modeling and control of multiphase machines – Part 1," *IEEE Trans. Ind. Electron.*, vol 63, no. 1, pp. 449–458, Jan. 2016.

[4] M.J. Duran and F. Barrero, "Recent advances in the design, modeling and control of multiphase machines – Part 2," *IEEE Trans. Ind. Electron.*, vol 63, no. 1, pp. 459–468, Jan. 2016.

[5] M.J. Duran, E. Levi, and F. Barrero, *Multiphase Electric Drives: Introduction*, Wiley Encyclopedia of Electrical and Electronics Engineering, pp. 1–26, 2017.

[6] H.S. Che, M.J. Duran, E. Levi, M. Jones, W.P. Hew and N.A. Rahim, "Post-fault operation of an asymmetrical six-phase induction machine with single and two isolated neutral points," *IEEE Trans. on Power Electron.*, vol. 29, no. 10, pp. 5406-5416, 2014

[7] I. Gonzalez-Prieto, M.J. Duran, F. Barrero, M. Bermudez and H. Guzman, "Impact of post-fault flux adaptation on six-phase induction motor drives with parallel converters," *IEEE Trans. on Power Electron.*, vol 32, no. 1, pp. 515-528, 2017.

[8] W. N. W. A. Munim, M. J. Duran, H. S. Che, M. Bermudez, I. González.-Prieto and N. A. Rahim, "A unified analysis of the fault tolerance capability in six-phase induction motor drives," *IEEE Trans.on Power Electron.*, vol. 32, no. 10, pp. 7824-7836, 2017.

[9] I. Gonzalez-Prieto, M.J. Duran and F. Barrero, "Fault-tolerant control of six-phase induction motor drives with variable current injection," *IEEE Trans. on Power Electron.*, vol. 32, no. 10, pp. 7894-7903, 2017

[10] F. Baneira, J. Doval-Gandoy, A. G. Yepes, Ó. López and D. Pérez-Estévez, "Control strategy for multiphase drives with minimum losses in the full torque operation range under single open-phase fault," *IEEE Trans.on Power Electron.*, vol. 32, no. 8, pp. 6275-6285, 2017.

[11] F. Baneira, J. Doval-Gandoy, A. G. Yepes, Ó. López and D. Pérez-Estévez, "Comparison of post-fault strategies for current reference generation for dual three-phase machines in terms of converter losses," *IEEE Trans. on Power Electron.*, vol. 32, no. 11, pp. 8243-8246, 2017.

[12] A. S. Abdel-Khalik, M. S. Hamad, A. M. Massoud and S. Ahmed, "Postfault operation of a nine-phase six-terminal induction machine under single open-line fault," *IEEE Trans. on Ind. Electron.*, vol. 65, no. 2, pp. 1084-1096, 2018.

[13] J. O. Estima and A. J. M. Cardoso, "A new approach for real-time multiple open-circuit fault diagnosis in voltage source inverters," *IEEE Trans. Ind. Applicat.*, vol. 47, no. 6, pp. 2487–2494, 2011.

[14] N. M. A. Freire, J. O. Estima, and A. J. M. Cardoso, "Open-circuit fault diagnosis in PMSG drives for wind turbine applications," *IEEE Trans. Ind. Electron.*, vol. 60, no. 9, pp. 3957–3967, 2013.

[15] W. Sleszynski, J. Nieznanski, and A. Cichowski, "Open-transistor fault diagnostics in voltagesource inverters by analyzing the load currents," *IEEE Trans. Ind. Electron.*, vol. 56, no. 11, pp. 4681–4688, 2009.

[16] J. O. Estima and A. J. M. Cardoso, "A new algorithm for real-time multiple open-circuit fault diagnosis in voltage-fed PWM motor drives by the reference current errors," *IEEE Trans. Ind. Electron.*, vol. 60, no. 8, pp. 3496–3505, 2013.

[17] F. Meinguet, E. Semail and J. Gyselinck, "An On-line Method for Stator Fault Detection in Multi-phase PMSM Drives," *in proc. of IEEE Vehicle Power and Propulsion Conference*, France, pp.1-6, 2010.

[18] M.J. Duran, I. Gonzalez-Prieto, N. Rios-Garcia and F. Barrero, "A simple, fast and robust open-phase fault detection technique for six-phase induction motor drives," *IEEE Trans. on Power Electron.*, vol. 33, no. 1, pp. 547-557, 2018.

[19] I. González-Prieto, M.J. Duran, N. Rios-Garcia, F. Barrero and C. Martín, "Open-switch fault detection in five-phase induction motor drives using model predictive control," *IEEE Trans.on Ind. Electron.*, vol. 65, no. 4, pp. 3045-3055, 2018.

[20] M. Bermudez, I. Gonzalez-Prieto, F. Barrero, H. Guzman, X. Kestelyn and M.J.Duran, "An experimental assessment of open-phase fault-tolerant virtual-vector-based direct torque control in five-phase induction motor drives," *IEEE Trans. on Power Electron.*, vol 33, no. 3, pp. 2774-2784, 2017.

[21] H. Guzman, M.J. Duran, F. Barrero, L. Zarri, B. Bogado, I. Gonzalez-Prieto and M.R. Arahal, "Comparative study of predictive and resonant controllers in fault-tolerant five-phase induction motor drives," *IEEE Trans. on Ind. Electron.*, vol. 63, no. 1, pp. 606-617, 2016.

[22] I. Gonzalez-Prieto, M. J. Duran, M. Bermudez, F. Barrero and C. Martin, "Assessment of Virtual-Voltage-based Model Predictive Controllers in Six-Phase Drives under Open-Phase Fault", *IEEE Journal of Emerging and Selected Topics in Power Electronics*, D.O.I: 10.1109/JESTPE.2019.2915666.

[23] I. Gonzalez-Prieto, M.J. Duran, P. Entrambasaguas and M. Bermudez, "Field Oriented Control of Multiphase Drives with Passive Fault-Tolerance," *IEEE Transactions on Industrial Electronics*, DOI: 10.1109/TIE.2019.2944056.

[24] A. Gonzalez-Prieto, I. Gonzalez-Prieto and M. J. Duran, "Efficient Predictive Control with Natural-Fault Tolerance for Multiphase Induction Machines," *IECON 2019-Lisbon*, 2019.

[25] P. Salas-Biedma, I. Gonzalez-Prieto and M. J. Duran, "Current Imbalance Detection Method based on Vector Space Decomposition Approach for Five-Phase Induction Motor Drives," *IECON 2019-Lisbon*, 2019.

[26] C. Xue, W. Song, and X. Feng, "Finite control-set model predictive current control of five-phase permanent-magnet synchronous machine based on virtual voltage vectors," *IET Electr. Power Appl.*, vol. 11, no. 5, pp. 836–846, May 2017.

[27] I. Gonzalez-Prieto, M.J. Duran, J.J. Aciego, C. Martin, and F. Barrero,"Model predictive control of six-phase induction motor drives using virtual voltage vectors," *IEEE Trans. Ind. Electron.*, vol. 65, no. 1, pp. 27–37, Jan. 2018.

[28] A. Yepes, J.A. Riveros, J. Doval-Gandoy, F. Barrero, O. Lopez, B. Bogado, M. Jones and E. Levi, "Parameter identification of multiphase induction machines with distributed windings-part 1: sinusoidal excitation methods," *IEEE Trans. on Energy Conv.*, vol. 27, no. 4, pp. 1056-1066, 2012.

Paula Garcia-Entrambasaguas was born in Málaga, Spain, in 1992. She received the University and Master's degrees in Industrial Engineering from the University of Málaga, in 2015 and 2017, respectively.
She is currently working toward the Ph.D. degree in the Electric Power Systems program at University of Málaga, Spain. Her research focuses on multiphase machines and drives and on control methods in pre- and post-fault situations.

Ignacio González-Prieto was born in Malaga, Spain, in 1987. He received the Industrial Engineer and M.Sc. degrees in fluid mechanics from the University of Malaga, Malaga, Spain, in 2012 and 2013, ´ respectively, and the Ph.D. degree in electronic engineering from the University of Seville, Sevilla, Spain, in 2016. His research interests include multiphase machines, wind energy systems, and electrical vehicles

[29] J.A. Riveros, A. Yepes, F. Barrero, J. Doval-Gandoy, B. Bogado, O. Lopez, M. Jones and E. Levi, "Parameter identification of multiphase induction machines with distributed windings-part 2: time-domain techniques," *IEEE Trans. on Energy Conv.*, vol. 27, no. 4, pp. 1067-1077, 2012.

Mario J. Duran was born in Bilbao, Spain, in 1975. He received the M.Sc. and Ph.D. degrees in electrical engineering from the University of Malaga, Malaga, in 1999 and 2003, respectively. He is currently a Full Professor in the Department of Electrical Engineering, University of Malaga. His research interests include modeling and ´ control of multiphase drives and renewable energies conversion systems.